Scattering of xenon from Ni(111): Collision-induced corrugation and energy transfer dynamics

Mark D. Ellison,[a] Carl M. Matthews, and Richard N. Zare
Department of Chemistry, Stanford University, Stanford, California 94305

(Received 19 April 1999; accepted 26 October 1999)

Experiments have been conducted in which a beam of xenon atoms collides with a clean Ni(111) surface, and the speed and angular distributions of the scattered Xe atoms are measured for different incident energies, incident angles, and surface temperatures. At high incident energies, the translational energy of the scattered Xe is independent of initial and final scattering angles. This result is attributed to multiple xenon-surface collisions prior to Xe escape. At lower incident energies, the scattering behavior depends more on the scattering angle. Interestingly, a small fraction of Xe is trapped on a 250 K Ni(111) surface at high incident translational energies. © *2000 American Institute of Physics.* [S0021-9606(00)70304-7]

I. INTRODUCTION

The scattering of rare gas atoms from surfaces is a well-researched field of study.[1] Of primary importance is the transfer of energy from the incident particle to the surface. The main energy transfer process at low-to-moderate collision energies is likely to be mechanical: specifically, either direct transfer of translational energy or indirect heating through increased vibrations in the environment of the incident atom. In a binary collision of two hard spheres, energy transfer is expected to be most efficient when the two atoms are comparable in mass. The presence of neighboring atoms at a surface complicates the collision, as they may increase the effective mass of the surface involved in the collision, or they may help dissipate the collision energy through phonons. Measuring the angular and velocity distributions of atoms scattered from a surface therefore helps to improve our understanding of the dynamics of the collision process. By use of seeded molecular beams and heated nozzles, such as Xe/H_2 at 2000 K, Xe atoms can be accelerated to energies up to 15 eV. This energy range is sufficient to probe diverse scattering behavior, including trapping, direct scattering, sputtering, and the breaking of chemical bonds at the surface.

The scattering of noble gas atoms from clean, close-packed metal surfaces has often been characterized in terms of conservation of momentum parallel to the surface.[1] This phenomenon has generally been attributed to a low corrugation in the gas-surface potential.[2] In the limit of a perfectly flat potential, the incident atom experiences no force directed in the surface plane, and the resulting velocity of the scattered atom exhibits an unchanged parallel momentum. Only momentum along the direction normal to the surface is exchanged with the surface. While many systems have been shown to deviate from this behavior at high incident energies,[3,4] conservation of parallel momentum typically becomes a better approximation of the scattering behavior of these systems at low incident energies. The reason is that if the atom approaches the surface with low kinetic energy, the turning point of the trajectory is relatively far from the surface where the corrugation of the potential is lessened. The opposite limit is a highly corrugated surface, on which parallel and perpendicular momenta are exchanged with equal facility.

Although much effort has been put into the investigation of rare gas atom-surface scattering,[3–7] most of these systems, such as Ar/Pt and Xe/Pt, are light/heavy combinations in which the gas atom has a smaller mass than the surface atom. Less is known about systems in which the gas atom is more massive than the surface atom. The scattering dynamics for such a heavy/light combination should be different, which motivated our investigation of the scattering of Xe from Ni(111).

II. EXPERIMENTAL APPARATUS

Our experimental apparatus incorporates a pulsed supersonic molecular beam that impinges upon a single-crystal surface in an ultrahigh vacuum (UHV) chamber. The scattered molecules are state-selectively ionized and detected by time-of-flight (TOF) mass spectrometry. By varying the time delay between the molecular beam pulse and the firing of the ionization laser, the velocity of incident and scattered atoms can be measured. A schematic of the experimental apparatus is shown in Fig. 1.

A. The molecular beam source

A pulsed nozzle (General Valve, 1 mm orifice) emits 300 μs long pulses at a repetition rate of 10 Hz. Approximately 1 cm downstream from the nozzle is a conical skimmer (Beam Dynamics, 0.49 mm orifice). The molecular beam is produced by seeding Xe (Praxair, 99.995% purity) in He (Matheson, 99.9995% purity) or Ar (Praxair, 99.9995% purity) and using a backing pressure of 50 psig. The nozzle and skimmer are located in a region of the chamber that is exhausted by a 10 in. diffusion pump (CVC PMC-10C), which achieves a typical base pressure of 5×10^{-7} torr. With the nozzle on, the pressure rises to 2×10^{-6} torr. After pass-

[a]Current address: Department of Chemistry, Wittenberg University, Springfield, OH 45501.

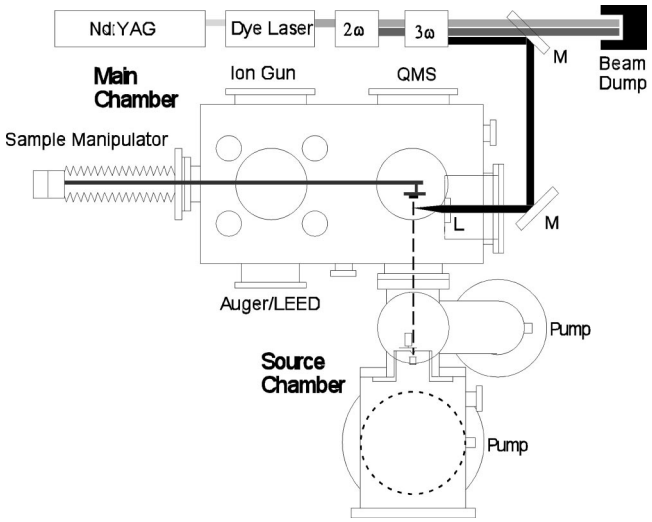

FIG. 1. Apparatus used in this experiment. Here QMS is the quadrupole mass spectrometer, M is mirror, and L is lens.

ing through the skimmer, the molecular beam is chopped by a rotating slotted disc. The chopper blade is a 0.75 mm thick aluminum disc with two diametrically opposed 0.75 mm wide slits. The chopper motor (Maxon) is capable of speeds greater than 300 revolutions per second. We found that 287 Hz is a good compromise between audible noise from the motor and a molecular beam pulse that is narrow enough temporally. A photoemitter/photodiode pair serves as the synchronization for the laser. A digital delay generator (SRS DG535) controls the delay between the nozzle fire and the Q-switch of the YAG laser. This configuration provides the least jitter in the time between the gas passing through the chopper slit and the firing of the laser. It produces a molecular beam pulse that is 15 μs in duration, as measured at the surface location. The translational temperature of the beam has been measured to be approximately 5 K. The chopper chamber is differentially pumped by a 6 in. diffusion pump (Varian VHS-6) and has a base pressure of 2×10^{-8} torr. After passing through the valve between the molecular beam and UHV chambers, the molecular beam passes through a collimating aperture 1 mm in diameter and about 15 cm from the surface. The beam diameter at the surface is measured to be 1 mm. With the molecular beam in operation, the pressure in the UHV chamber rises by 2×10^{-11} torr.

B. The main ultra-high vacuum (UHV) chamber

The UHV vacuum chamber is pumped by a liquid-nitrogen-trapped 10 in. diffusion pump (Edwards E012), achieving a base pressure of 1.5×10^{-9} torr. Surface cleanliness and order are monitored using a reverse-view low-energy electron diffraction (LEED)/Auger spectrometer (Fisons RVL 900) after sputtering by an ion gun (Varian). The sample is mounted on a manipulator with three translational degrees of freedom and two independent angular rotations (Vacuum Generators). The sample holder may be rotated 360° about the manipulator shaft, and the crystal may be tilted $\pm70°$ about an axis parallel to its surface. In practice, however, we found that we could not perform experiments at incident angles greater than $\sim40°$, owing to design limitations in the manipulator. A filament behind the sample plate heats the sample to temperatures above 1300 K, as monitored by a chromel-alumel thermocouple spot-welded to the front face of the crystal. The thermocouple reading was checked against an optical pyrometer and found to be accurate to within 5 K. Using Auger electron spectroscopy, we observed that the surface remains free of contaminants for many hours if held above 800 K, but only for about 2 h if the temperature of the sample was below 500 K. Thus, for the studies at low temperature, we found it necessary to sputter and anneal the surface to remove contaminants prior to each scattering experiment.

The Ni(111) crystal (Aremco Products) was taken from a boule of 99.9995% purity and cut to within $\pm0.5°$ of the (111) face. Sulfur, carbon, oxygen, and a small amount of calcium were the major contaminants. They were painstakingly removed after roughly 800 h of sputtering with 500 eV argon ions at a surface temperature of 1000 K. Once most of the contaminants were removed, the daily cleaning procedure was to sputter with 500 eV argon ions at a surface temperature of 1000 K for 30 min, followed by 30 min of annealing at 1000 K. This procedure consistently produced a clean surface as measured by Auger electron spectroscopy (AES), with contaminant levels below the 1 detection limit. Furthermore, low-energy electron diffraction (LEED) patterns showed very sharp (1×1) spots and little diffuse background.

C. The laser ionization/time-of-flight (TOF) detector

To detect the Xe, we used a $(2+1)$ resonantly enhanced photon ionization (REMPI) process via the $5p^5 9f$ Rydberg state. The light required for the ionization, at a wavelength of approximately 210 nm, is generated in the following manner. The second harmonic of a pulsed Nd:YAG laser (Continuum NY61-10) pumps a tunable dye laser (Lambda Physik Scan-Mate 2E) to produce light at about 630 nm. An angle-tuned BBO crystal (Inrad Autotracker II) produces the second harmonic of the dye laser output, and the residual dye fundamental and harmonic are mixed in a second angle-tuned BBO crystal (Inrad Autotracker II). The dye laser output of 60 mJ at 630 nm results in 12 mJ at 315 nm and 1 mJ at 210 nm. The 210 nm light is separated from the other wavelengths by dichroic mirrors (Virgo Optics) and focused into the chamber with an uncoated 200 mm lens (CVI Optics). The final two dichroics and the lens are mounted on linear translation stages (Newport) actuated by manual micrometers, which allows the laser focal volume to be accurately positioned in front of the surface. The laser focus is truly a volume as opposed to a ''dimensionless'' spot. We estimate that our beam waist at the focus is no smaller than 20 μm. From this, we calculate a confocal parameter[8] of 1.2 cm, from which we estimate that we ionize out-of-plane scattered Xe at least out to 20° on either side of the scattering plane. Our data, then, represent a projection of some of the out-of-plane scattered Xe onto the scattering plane.

The scattered molecules are steered into a time-of-flight tube by ion optics; at the end of the tube they strike a 40 mm multichannel plate array (R. M. Jordan Co.). The MCP signal

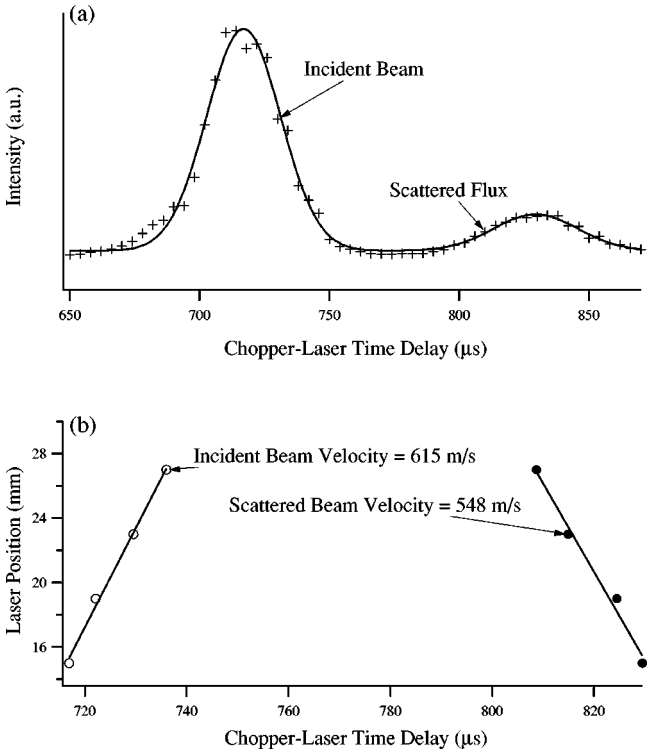

FIG. 2. (a) The TOF spectrum of Xe atoms incident along the surface normal on a clean, 1000 K Ni(111) surface. The *x* axis indicates the time delay from the opening of the chopper to the firing the laser. The peak on the left is the incident beam. The peak on the right corresponds to Xe atoms that have scattered along the surface normal. (b) Surface position calibration plot. The shift in the time of the peak of the incident and scattered atoms is recorded as a function of laser position. The position of the surface is calculated by extrapolating the peak position of the incident and scattered flux to their intersection.

is averaged in a digital oscilloscope and acquired by a desktop computer (Macintosh Quadra 950) for storage and analysis. Control of the laser and data acquisition is achieved using a self-written program under LabView (National Instruments).

The velocities of the incident molecular beam and the scattered atoms are measured by translating the laser in front of the surface using the micrometer-driven translation stage described above. This arrangement has been successfully utilized to measure the scattered velocities and angular distributions for other gas-surface systems, including N_2/Cu(110),[9,10] H_2/Cu(110),[11] and H_2/Pd(111).[12] The delay time corresponding to the peak ion signal is recorded, and the process is repeated at various locations in the direction of propagation of the molecular beam. If the surface is perpendicular to the molecular beam, then the atoms that scatter straight back along the surface normal are also detected, as shown in Fig. 2(a). In this manner, the velocities of both the incident beam and the Xe atoms that scatter directly back along the surface normal can be measured. A plot of the laser micrometer reading versus the delay time corresponding to maximum ion intensity yields a line whose slope is the most probable velocity. An example of this analysis is shown in Fig. 2(b). Because both the incident and directly scattered atoms have a symmetric peak shape, the most probable velocity can be directly converted into a mean kinetic energy. This method is quite accurate. The major source of uncertainty is 5% or less, which arises from the calibration of the surface position.

In addition to the velocity measurements, angular distributions of the scattered Xe were also measured. In these experiments, the laser focal volume is translated in front of the surface in 5° increments at a constant distance, typically 1.5–2 cm, from the intersection area of the molecular beam with the surface. At this distance, the in-plane angular resolution of our measurements is 3° to 5°. This procedure yields the intensity of the scattered Xe at various angles.

When the angular distributions were collected, the laser-chopper delay was set to yield maximum ion signal. As will be presented below, the temporal distribution of scattered atoms contains contributions both from atoms that have directly scattered and from those that have been trapped on and subsequently desorbed from the surface. Because these two contributions overlap, our angular distributions can indicate either type of behavior, or both. Our angular distributions are, therefore, most useful in determining which type of behavior, direct inelastic scattering or trapping/desorption, dominates under the given experimental conditions.

Because the collection efficiency of the detector is not constant for all scattering angles, we found it necessary to correct for that variation in the following manner. Xe gas is introduced into the chamber via a leak valve so that a uniform pressure of Xe exists throughout the detection region. The ion signal from the Xe at various laser positions is then detected. Because the Xe background is uniform, this ion signal reflects the detector efficiency as a function of scattering angle. The ion signal from the scattered Xe is then divided by the ion signal from the Xe gas at the same point in space. The procedure works best if the detection efficiency does not vary rapidly across the range of scattering angles probed. Fortunately, we were able to find voltages for the ion optics that satisfy this requirement.

III. RESULTS

A. Angular distributions

Angular distributions and most probable velocities for the scattering of Xe from Ni(111) have been measured as a function of incident angle, incident energy, and surface temperature. In particular, for two different incident kinetic energies, 0.26 and 1.8 eV, velocity and angular distributions have been measured for incident angles of 0° and 20° at surface temperatures of both 250 and 1000 K.

The angular distributions for normally incident 1.8 eV Xe scattered from a Ni(111) surface at surface temperatures of 250 and 1000 K, are shown in Fig. 3(a). At both temperatures, a narrow scattering lobe centered around the surface normal is observed. These distributions are consistent with direct inelastic scattering, which is expected to dominate over trapping/desorption for the Xe/Ni(111) system under these conditions. The width of the lobe narrows slightly as the temperature decreases. In particular, at normal incidence the full width at half-maximum (FWHM) of the scattered distribution at a surface temperature of 250 K is 15°, whereas at 1000 K it is 25°. The broadening of the distribu-

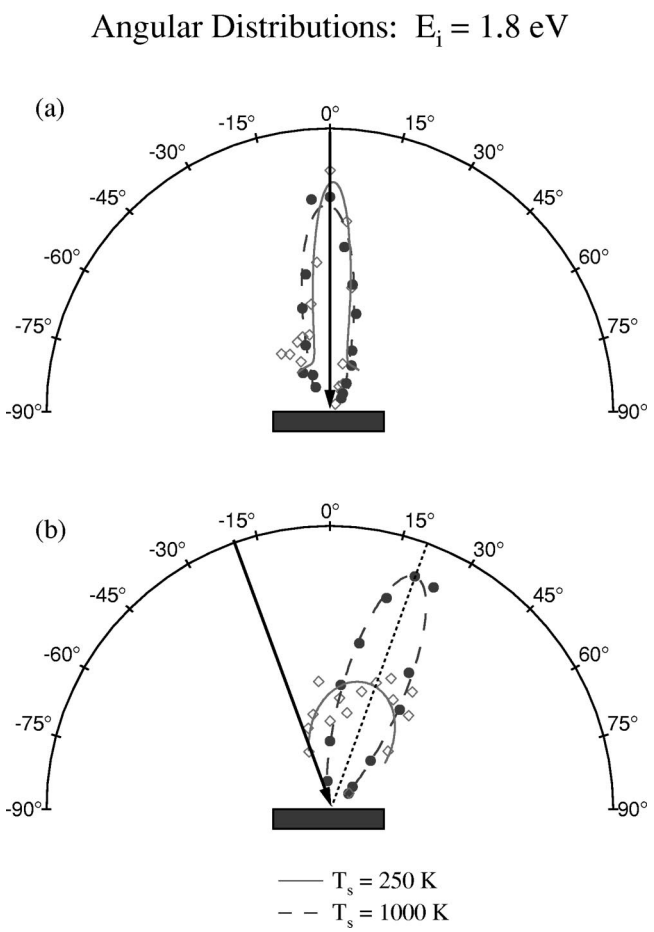

FIG. 3. Angular distributions for 1.8 eV Xe scattered from a clean Ni(111) surface. The graphs are polar plots with the radius from the surface indicating the intensity of Xe at each angle. The curves are fits to guide the eye. The incident angle is indicated by an arrow, and the specular direction is indicated by a heavy dashed line. On the clean surface at normal incidence (a), the scattered distribution is a narrow lobe, indicating direct inelastic scattering. At 20° incidence (b), the colder surface has a much wider peak, indicating some trapping occurs.

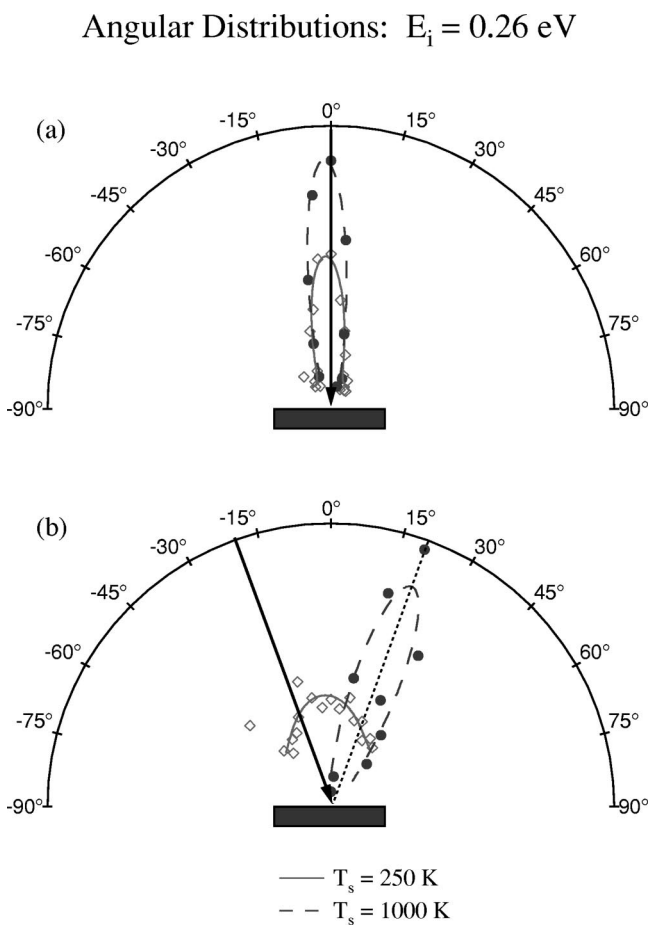

FIG. 4. Angular distributions for 0.26 eV Xe scattered from a clean Ni(111) surface. On the clean surface at normal incidence (a), the scattered distribution indicates direct inelastic scattering. At 20° incidence (b), the colder surface has a broad peak directed toward the surface normal.

tion at higher surface temperature is thought to be caused by thermal motion of the surface atoms. The higher the surface temperature, the greater the displacement of the surface atoms from their equilibrium positions. As a result, the surface appears rougher to the Xe atoms, which then scatter into a wider range of exit angles. Thus, the scattering behavior of Xe from Ni(111) must be more complex than simple specular reflection from a hard, smooth surface.

The angular distributions for 20° incidence at 1000 K surface temperature [Fig. 3(b)] also indicate direct inelastic scattering. At 20° incidence, the scattered distribution for the higher surface temperature is again a narrow lobe that peaks at the specular angle.

At off-normal incidence and a surface temperature of 250 K, as shown in Fig. 3(b), the scattering behavior is quite different. Instead of a purely lobular distribution, the scattered intensity is more diffuse, with a peak toward the specular direction but also with significant intensity over a wide range of angles. Because our angular distribution data are sensitive to atoms that have directly scattered and to those that have been trapped and have been subsequently desorbed, this result suggests that a trapping/desorption process is important under conditions in which the incident Xe atoms become temporarily bound to the surface. This interpretation of trapping, based on the angular distributions, is also supported by the velocity measurements presented below.

Figures 4(a) and 4(b) show the scattered Xe angular distributions for 0.26 eV incident translational energy at incident angles of 0° and 20°. It is seen that the angular distributions change markedly when the incident energy is lowered to 0.26 eV. The well depth for this system, determined by Wong and Zhu,[13] is 0.2 eV. Under these conditions, the Xe atoms have an incident kinetic energy of a comparable magnitude to the well depth. Thus, the scattering behavior is expected to be significantly different from the behavior of atoms that have an incident energy much greater than the well depth.

For normal incidence, as with the high incident energy result for normal incidence, the scattering distributions at surface temperatures of 250 and 1000 K both show in Fig. 4(a) a narrow lobe centered at the surface normal. However, in contrast to the high incident energy angular distribution, the FWHM of the scattered distribution increases from 16° at a surface temperature of 1000 K to 21° at a surface temperature of 250 K. A decrease in the surface atom motion at lower temperatures should lead to a narrower angular distri-

bution. However, if trapping/desorption contributes significantly to the signal, an angular distribution is expected with a large cosine-like component on top of a narrower peak from direct inelastic scattering. Based on this angular distribution, we expect to observe some trapping/desorption for 0.26 eV Xe incident upon a 250 K Ni(111) surface.

Figure 4(b), the scattered angular distributions for 0.26 eV Xe incident at 20°, also indicates that trapping has become more important at low incident energies. The scattering from the 1000 K surface indicates direct inelastic scattering, with a narrow lobe centered about the specular, but the scattering from the 250 K surface has an angular distribution that is very broad and centered about the surface normal, typical of a trapping/desorption feature.

B. Velocity distributions

The velocity distributions of scattered Xe atoms were determined for each of the incident conditions described above. In general, the temporal width of the directly scattered atoms' TOF distribution is only slightly greater than the width of the incident peak. Therefore, no information other than the most probable velocity (such as a surface residence time) can be extracted from the scattered atoms. The maximum of the TOF signal represents the most probable velocity, and from this velocity the most probable kinetic energy of the scattered atoms can be directly calculated. Figures 5(a) and 5(b) show the ratio of the scattered kinetic energy to the initial kinetic energy as a function of scattering angle for incident angles of 0° and 20° at 1.8 eV incident energy, respectively. For each incident angle studied, the energy ratio remains nearly constant over the entire range of scattering angles, including the case of 40° incidence. Also shown in Fig. 5(b) is the prediction of parallel momentum conservation, which clearly breaks down as an approximate description of the scattering of Xe from Ni(111). Thus, the data is Fig. 5 gives further evidence that the scattering environment of the Xe atom is highly corrugated.

The raw velocity data for Xe scattered from the 250 K surface are quite different than those for Xe scattered from the hotter surface. As shown in Fig. 6, the TOF peak is asymmetric, with a tail extending to long flight times. This tail is not present in the scattering from the hot surface and is not an artifact of the molecular beam expansion. As shown in the inset, the relative size of the tail is different for different scattering conditions. In combination with the broad angular distributions discussed above, the tail on the velocity data strongly suggests a trapping/desorption process. By this hypothesis, the velocity data were least-squares fit by a function that is the sum of a Gaussian component and a general TOF distribution.[14] Because our detection system measures the gas *density*, the form of the TOF distribution used is $f(t) \propto t^{-4} \exp[-[(x/t - v_o)/\alpha]^2]$, where x is the flight distance, v_o is the stream velocity, and α is the width of the peak. If the distribution is at thermal equilibrium, then $v_o = 0$ and $\alpha = (2kT/m)^{1/2}$, where T is the temperature of the gas and m the mass. The Gaussian part of the fit reflects the direct scattering process. The Gaussian function was chosen because it describes well the incident molecular beam peak and because the direct inelastic scattering does not change the shape of the curve to any appreciable extent. The TOF distribution was selected because it is general enough to fit extremes in velocity behavior ranging from supersonic beam expansions to Maxwell–Boltzmann distributions.

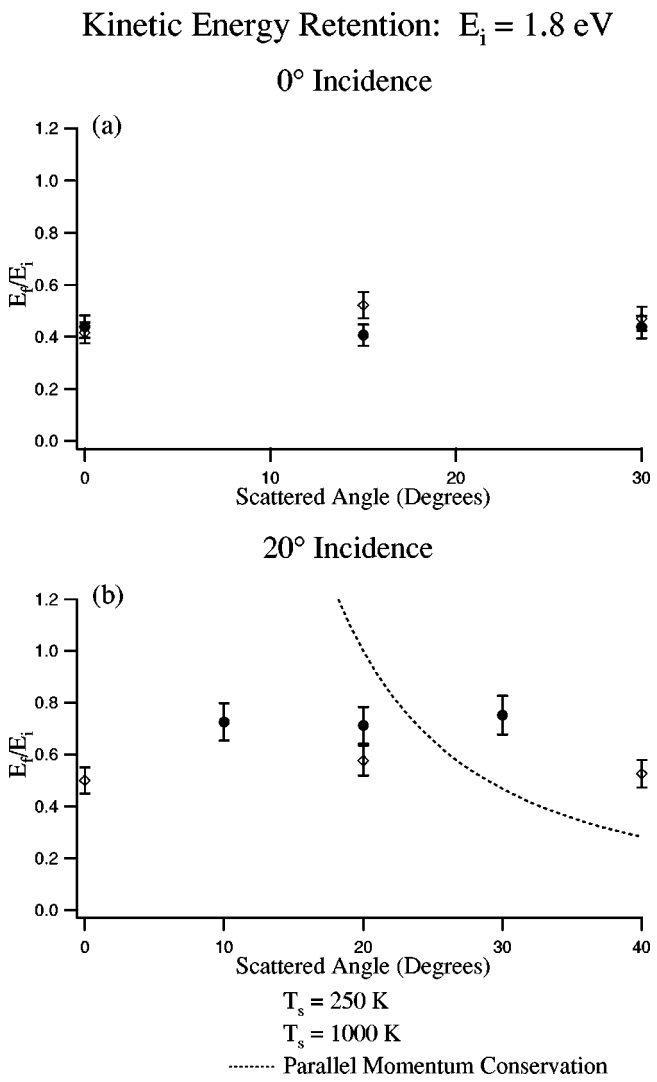

FIG. 5. Ratio of scattered kinetic energy to initial energy for 1.8 eV Xe from a clean Ni(111) surface as a function of final scattering angle. All of the kinetic energy curves show little dependence on exit angle. The dashed line shows the prediction of final kinetic energy with parallel momentum conservation. Xe atoms scattered from the 1000 K surface have a higher energy than those scattered from the 250 K surface.

In keeping with previous investigations, the most probable direct scattering velocity is calculated using the peak of the Gaussian component. In contrast, the asymmetric portion of the distribution to longer flight times that is fit with the general TOF distribution represents the atoms that have undergone a longer interaction with the surface. Thus, we have the ability to separate the direct inelastic scattering channel from the trapping/desorption channel, although some overlap is present. Because the incident atoms that are trapped equilibrate with the surface on a time scale of tens of picoseconds, trapped Xe atoms, although they may have had a very short stay on the surface, should be traveling much more slowly than directly scattered atoms. As both scattered and trapped atoms traverse the distance between the surface and the laser

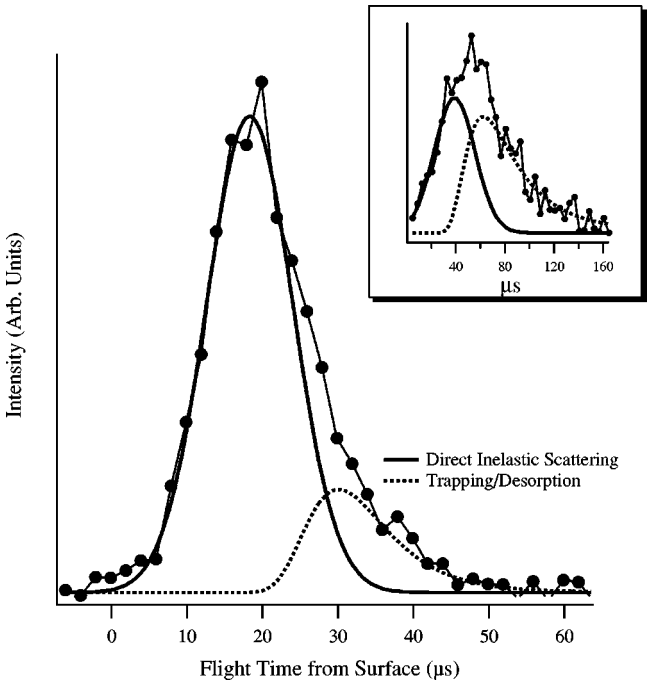

FIG. 6. Raw TOF data of Xe scattered from clean Ni(111). These data were taken at 1.8 eV, normal incidence, 30° detection. The peak is cleanly divided into a direct scattering part and a trapping/desorption part. A comparison of the area under the two curves gives an estimate of the amount of trapping/desorption at this exit angle. The inset shows an example curve taken at 0.26 eV, 20° incidence, 30° detection. Increased trapping occurs under these conditions.

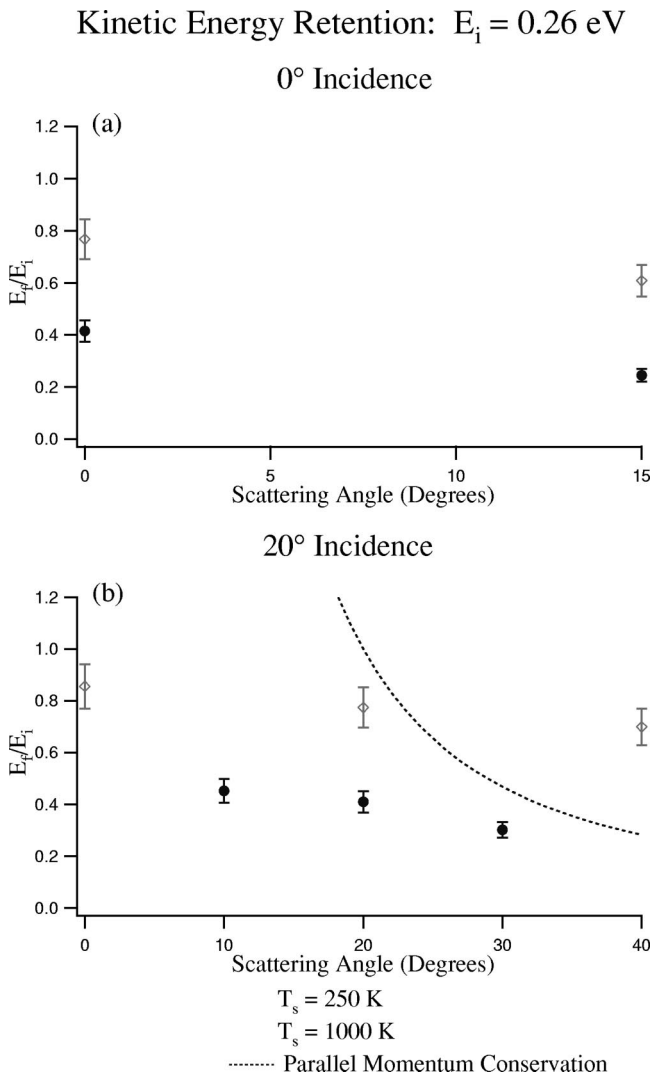

FIG. 7. Ratio of scattered atom kinetic energy to initial energy for 0.26 eV Xe from a clean Ni(111) surface as a function of final scattering angle. The kinetic energy refers to the energy of the direct inelastic scattering peak. Each of the kinetic energy curves show a slight dependence on exit angle. Xe atoms scattered from the 1000 K surface have a lower energy than those scattered from the 250 K surface.

focal volume, the two channels should separate sufficiently in time so that they can be resolved in our TOF data. Thus, in comparing scattered energies at different angles and surface temperatures, we are confident that the quantity we report as scattered kinetic energy, which is obtained from the Gaussian part of the fit to the data, has little, if any, contribution from atoms that have been trapped by the surface and subsequently have been desorbed from it.

Using this analysis procedure, the best-fit TOF distribution yields, at all incident and scattering angles, a translational temperature of 250 ± 50 K. The large uncertainty is caused by the uncertainty in arrival time at the surface and the uncertainty in the distance from the laser to the surface. From these results, we conclude that even at high incident kinetic energies a small fraction of the incident Xe atoms are trapped on a cold Ni(111) surface.

In addition to direct inelastic scattering, a significant trapping/desorption peak was also observed for 0.26 eV Xe incident upon a clean 250 K Ni(111) surface, as shown in Figs. 7(a) and 7(b). In fact, at each incident angle, the TOF distribution data reveal an overall enhancement of trapping. This increase in trapping at a lower incident kinetic energy is not surprising and has been observed for several systems, such as Ar/Pt(111),[15,16] Ar/2H–W(100),[17] and Xe/Pt(111).[18,19] Our data indicate that this trend also holds for Xe/Ni(111).

IV. DISCUSSION

A. Collision-induced corrugation of Ni(111)

The scattering of Xe from the Ni(111) surface exhibits a complex behavior that is dependent upon the Xe incident kinetic energy, Xe incident angle, and surface temperature. The most striking observation is the near-independence of the energy transfer with respect to both incident and final angles. For 1.8 eV incident Xe, the velocity distributions have no dependence on the exit angle of the scattered Xe atom (Fig. 5). As the energy is lowered to 0.26 eV, a weak dependence of the final velocity on the exit angle is evident (Fig. 7). This dependence does not closely approximate parallel momentum conservation, in spite of the fact that the amount of corrugation would be expected to be significantly smaller owing to the lower collision energy.

Our data are dissimilar to the results for the scattering of Ar from Ag(111),[3,7,20] and Xe from Pt(111).[4] In these two

systems, incident energies of approximately 2 eV resulted in scattered energies that were independent of scattered angle. As the incident energy was lowered to less than 1 eV, parallel momentum conservation was observed. Such behavior has been described as a transition from structure scattering to thermal scattering.[21] At high incident energies, the impinging atoms penetrate more deeply into the repulsive part of the gas-surface potential, so the structure of the surface is the dominant factor in determining the scattering behavior. At low incident energies, the thermal motion of the surface atoms becomes important, so that the surface appears flat except for the relatively small displacements of the surface atoms about their equilibrium positions. In contrast to the results of the Ar/Ag(111) and Xe/Pt(111) studies, our data clearly reveal that the interaction potential between Xe and the Ni(111) surface is corrugated owing to disruption of the surface lattice and the necessity of multiple collisions even at the low incident energy of 0.26 eV. Although the corrugation induced by the Xe atom's impact is smaller at low incident energies, the low incident energy is still sufficient to cause evidently some short-range buckling of the lattice.

The angular distribution data further confirm that collision-induced corrugation plays a part in the scattering dynamics. Because trapping is expected to be negligible for a surface temperature of 1000 K, the FWHM of the angular distribution can be a guide to the amount of corrugation in the surface potential. For normal incidence and a surface temperature of 1000 K, the FWHM of the scattered angular distribution is 25.5° for 1.8 eV incident Xe (Fig. 3), but only 16.0° for 0.26 eV Xe (Fig. 4). Similarly, the FWHM of the angular distributions for off-normal incidence changes as the incident energy is decreased. For 20° incidence and scattering from a 1000 K surface, the FWHM drops from 27.3° [Fig. 3(b)] to 20.9° [Fig. 4(b)] as the incident energy decreases from 1.8 to 0.26 eV. This narrowing of the angular distribution as the incident energy decreases suggests that the surface corrugation decreases as the incident energy drops from 1.8 to 0.26 eV. In essence, the angular distribution FWHM measurements are in accord with a transition from structure to thermal scattering, indicating that as the incident kinetic energy is decreased, the thermal motion of the surface atoms plays a greater role in determining the scattering angle.

In addition to the FWHM of the angular distributions, the direction of the peak of the angular distribution also includes information about the scattering dynamics. A common feature of all of the angular distributions we obtained that exhibit direct inelastic scattering is that the peak of the distribution is always at or below the specular angle. This observation differs from earlier results obtained by Rettner, Barker, and Bethune[4] on the Xe/Pt(111) system. They observed superspecular scattering under comparable conditions (incident angles of 30° and 40°, incident energies of 1.17 and 0.5 eV, and a surface temperature of 800 K). Raukema, Dirksen, and Kleyn[3] found that Ar incident on Ag(111) scatters slightly to the superspecular at surface temperatures from 330 to 800 K with an incident angle of 40° and an incident energy of 1.06 eV. The same behavior is observed for incident energies from 0.21 to 2.56 eV at a surface temperature of 600 K. Although velocity distributions are needed for confirmation, these results are often indicative of a smooth, flat potential. Upon impact with the surface, the atom loses perpendicular momentum to the surface and conserves parallel momentum. For an atom to scatter subspecularly with parallel momentum conservation, it must gain energy from the surface. The Xe/Ni(111) system does not conform to these expectations, as the scattered Xe atoms are observed to lose energy to the surface at all scattering angles. The subspecular scattering observed for Xe/Ni(111) further confirms the breakdown of parallel momentum conservation.

The inclusion of parallel momentum in the scattering dynamics is necessary to describe the scattering dynamics. The most straightforward explanation invokes corrugation of the surface to accomplish this. If the adsorption well were relatively deep, then the corrugation across the unit cell could be substantial. The well depth for Xe/Ni(111) has been investigated by Wong and Zhu,[13] and they determined the barrier to desorption to be 4.4 kcal/mol (0.19 eV) in an isothermal optical differential reflectance experiment. However, Fargues *et al.*[22] measured an isosteric heat of adsorption at 7.3 kcal/mol (0.32 eV). Wong and Zhu suggest that the difference arises from a higher defect density in the sample of Fargues *et al.* because the cut of the crystal used in the experiments of Fargues *et al.* (1°) had greater uncertainty than the cut of Wong and Zhu's crystal (0.1°). Wandelt and Hulse[23] have observed the following energetic trend on another fcc metal, Pd: $E_{\mathrm{des}}(111) < E_{\mathrm{des}}(100) < E_{\mathrm{des}}(110)$. Assuming the trend holds generally for fcc metals and using $E_{\mathrm{des}} = 5.2$ kcal/mol found by Christmann and Demuth[24] on Ni(100), the lower value of the desorption energy determined by Wong and Zhu for Ni(111) seems more reasonable. This small well depth suggests that the lateral variation in the gas-surface potential is quite small. If the static corrugation, then, is too small to reasonably account for the observed near independence of the final energy on scattered angle, another explanation for the corrugation must be found.

Given that the adsorption well for the Xe/Ni(111) system is relatively shallow, the corrugation that gives rise to the observed near independence of the scattered atom's velocity on exit angle is unlikely to occur when the surface atoms are near their equilibrium positions. Therefore, the corrugation must be caused by a process that moves the surface atoms away from their ''static'' equilibrium positions. Although the angular distribution data show that the thermal motion of the surface atoms does affect the scattering behavior, we do not believe that this motion is sufficiently large to be responsible for the observed energy dependence on scattered angle. The displacement of Ni surface atoms about their equilibrium positions is only 0.2–0.3 Å at the surface temperatures studied here. The corrugation manifested in the scattered kinetic energies is far more likely to be induced by the impact of the Xe atom. The impact of the Xe atom drives the Ni atom closest to the Xe atom into the surface, and the neighboring Ni atoms are also dragged along to different degrees. Furthermore, the mismatch between the mass of a Xe atom and the effective mass of the Ni surface is important in this process. The mismatch is sufficiently large that an incident Xe atom will undergo at least two collisions with the surface.

A surface interaction that requires at least two collisions is certainly more complex and more likely to cause disruption of the surface lattice than a single collision with a smooth, flat surface. Indeed, the invocation of corrugation to explain the scattering behavior implies that the Xe atom collides with multiple surface atoms during the course of the collision event. As the massive Xe atom collides with the Ni(111) surface, the atom causes a significant local distortion of the normally flat surface. After the initial impact, the Xe more or less continues in its initial direction, likely creating a small ''pocket'' of nearby Ni atoms. This buckling of the surface provides a corrugated scattering environment, because the Xe atom probably collides with several Ni atoms around it before escaping from the surface. The presence of nearby Ni atoms in locations other than ''under'' the Xe atom increase the likelihood of exchange of parallel and normal momentum, resulting in the breakdown of parallel momentum conservation that we observe.

The distortion of the Ni(111) surface by the Xe atom has been observed in other experiments. Ceyer and co-workers[25] have shown that at higher energies (5–10 eV), noble gas atoms (Ar, Kr, and Xe) will displace the atoms at the same surface to such an extent as to allow preadsorbed H atoms to migrate into the bulk Ni. Given this observation, a lesser buckling of the surface at the incident energies we studied, sufficient to result in a corrugated scattering environment, seems reasonable.

Finally, the scattering dynamics can also be used to elucidate the adsorption process. The observation of both direct inelastic scattering and trapping/desorption for Xe/Ni(111) is similar to the behavior of Xe scattered from Pt(111). Hurst *et al.*[26] found that Xe incident on a Pt(111) surface displays both direct inelastic scattering and trapping/desorption. In fact, our decomposition of the overall scattered intensity into two distinct channels is based on their treatment of similar TOF data. However, their experimental conditions—75° incidence, a surface temperature of 185 K (although trapping was observed at a surface temperature as high as 373 K), and incident energies below 0.14 eV—should enhance trapping. In contrast, the higher incident energy and surface temperature used in our experiments should decrease the amount of trapping. Despite the differences in experimental conditions, the ability to distinguish between direct inelastic scattering and trapping/desorption is a common characteristic of both experiments.

Figures 7(a) and 7(b) show an unexpected yet consistent trend: at all incident angles for 0.26 eV incident Xe, the fractional energy retention of directly scattered atoms is always greater for scattering from a 250 K surface than for scattering from a 1000 K surface. This observation is counterintuitive because energy from a hot gas should be more easily deposited into a cold body than into a hot body. We believe that this unexpected behavior is explained in terms of the trapping of Xe atoms at the Ni(111) surface at 250 K. Because these data represent the Xe atoms that have directly scattered, these Xe atoms must have sufficient kinetic energy to escape the potential well. In order to avoid becoming trapped, the Xe atoms must retain a large fraction of their incident kinetic energy because this energy is only slightly larger than the well depth.

The trapping of Xe at a clean 250 K Ni(111) surface may be facilitated by the occurrence of multiple collisions. In its initial collision the Xe atom strikes one or more Ni atoms, pushing them toward the bulk, but continues in toward the surface. If the Ni atoms rebound with sufficient kinetic energy, they will strike the Xe atom and cause it to reverse direction. If the kinetic energy imparted to the Xe is greater than the well depth, then the Xe will escape from the surface. But if the Ni atoms are efficient in transferring to the neighboring atoms the energy they received from the Xe atom, then the Ni atoms will be unlikely to give the Xe a sufficient kick in the second collision to cause the Xe to leave the surface. A Ni atom with a kinetic energy appropriate for the surface temperature of 250 K is unlikely to give the Xe atom sufficient kinetic energy to escape the gas-surface well.

In conclusion, the 0.26 eV incident Xe data show an enhancement of trapping at 250 K over the 1.8 eV incident Xe. The scattered angular distributions indicate more diffuse scattering, caused by increased interaction with the surface. The velocity data show that the 1000 K surface decreases retention of the incident kinetic energy after scattering. The amount of trapping at 0.26 eV incident energy appears to be greater than the amount of trapping at 1.8 eV incident energy, which is in good agreement with measurements performed on other noble gas atom-metal surface systems. Finally, a comparison of 1.8 eV incident Xe with 0.26 eV incident Xe scattered from a 250 K Ni(111) surface demonstrates that the scattering behavior approaches parallel momentum conservation as the incident energy decreases. However, the data still deviate significantly from this behavior because the mass of the Xe requires lattice deformation and at least two gas-surface collisions.

V. CONCLUSIONS

From previous studies of rare gas atoms scattering from well-defined surfaces, it might be expected that the scattering of Xe from a clean, close-packed Ni(111) surface would be rather straightforward to interpret. We find instead that this system displays a complex and unexpected scattering behavior. Parallel momentum conservation does not even approximately describe the complete scattering dynamics from a 1000 K surface. We interpret this result as indicating that the incident Xe atom is too massive to be reflected into the gas phase by a single collision with the surface. Instead, the Xe atom causes a local lattice distortion in the area of the collision, which creates a rather corrugated environment for the Xe. As expected, the extent of the lattice deformation decreases as the incident kinetic energy of the Xe decreases. Consequently, the scattering behavior of Xe scattered from Ni(111) departs from independence of the scattered energy with scattered angle as the incident translational energy decreases from 1.8 to 0.26 eV. Conservation of parallel momentum still does not hold at 0.26 eV incidence energy, primarily because the mass of the Xe atom causes multiple collisions with the surface to occur before the Xe atom is able to escape from the surface.

The angular and velocity distributions of Xe atoms scattered from a 250 K Ni(111) surface demonstrate that some Xe is trapped under these conditions. The observation of trapping at this surface temperature is surprising, especially at 1.8 eV incidence, given the low binding energy of Xe to Ni(111), which is estimated to be 0.19 eV. Trapping at 0.26 eV incident energy is increased over trapping at 1.8 eV incidence, in good agreement with other work on noble gas-metal systems.

ACKNOWLEDGMENTS

The authors gratefully acknowledge Greg Sitz for several useful discussions regarding Auger electron diffraction features and Dan Auerbach for critical discussions of the paper. One of the authors (C.M.M.) acknowledges support by the Hertz Foundation. We thank the Office of Naval Research (Grant No. N00014-91-J-1023) and the National Science Foundation (Grant No. CHE-9900305) for support of this work.

[1] J. A. Barker and D. J. Auerbach, Surf. Sci. Rep. **4**, 1 (1984).
[2] M. Head-Gordon and J. Tully, Surf. Sci. **268**, 113 (1992).
[3] A. Raukema, R. J. Dirksen, and A. W. Kleyn, J. Chem. Phys. **103**, 6217 (1995).
[4] C. T. Rettner, J. A. Barker, and D. S. Bethune, Phys. Rev. Lett. **67**, 2183 (1991).
[5] A. Amirav, M. J. Cardillo, P. L. Trevor, C. Lim, and J. C. Tully, J. Chem. Phys. **87**, 1796 (1987).
[6] F. O. Goodman and H. Y. Wachman, *Dynamics of Gas-Surface Scattering* (Academic, New York, 1976).
[7] R. J. W. E. Lahaye, A. W. Kleyn, S. Stolte, and S. Holloway, Surf. Sci. **338**, 169 (1995).
[8] A. E. Siegman, *Lasers* (University Science Books, Mill Valley, 1986).
[9] J. L. W. Siders and G. O. Sitz, J. Chem. Phys. **101**, 6264 (1994).
[10] J. L. W. Siders and G. O. Sitz, J. Vac. Sci. Technol. A **13**, 1400 (1995).
[11] M. Gostein, H. Parhikhteh, and G. O. Sitz, Phys. Rev. Lett. **75**, 342 (1995).
[12] M. Gostein, E. Watts, and G. O. Sitz, Phys. Rev. Lett. **79**, 2891 (1997).
[13] A. Wong and X. D. Zhu, Appl. Phys. A: Mater. Sci. Process. **63**, 1 (1996).
[14] H. Haberland, U. Buck, and M. Tolle, Rev. Sci. Instrum. **56**, 1712 (1985).
[15] C. B. Mullins, C. T. Rettner, D. J. Auerbach, and W. H. Weinberg, Chem. Phys. Lett. **163**, 111 (1989).
[16] M. Head-Gordon, J. C. Tully, C. T. Rettner, C. B. Mullins, and D. J. Auerbach, J. Chem. Phys. **94**, 1516 (1991).
[17] C. T. Rettner, E. K. Schweizer, and C. B. Mullins, J. Chem. Phys. **90**, 3800 (1989).
[18] C. R. Arumainayagam, J. A. Stinett, M. C. McMaster, and R. J. Madix, J. Chem. Phys. **95**, 5437 (1991).
[19] C. T. Rettner, D. S. Bethune, and D. J. Auerbach, J. Chem. Phys. **91**, 1942 (1989).
[20] H. Asada and T. Matsui, Jpn. J. Appl. Phys. **21**, 259 (1982).
[21] R. A. Oman, J. Chem. Phys. **48**, 3919 (1968).
[22] D. Fargues, P. Dolle, M. Alnot, and J. J. Ehrhardt, Surf. Sci. **214**, 187 (1989).
[23] K. Wandelt and J. E. Hulse, J. Chem. Phys. **80**, 1340 (1984).
[24] K. Christmann and J. E. Demuth, Surf. Sci. **120**, 291 (1982).
[25] K. J. Maynard, A. D. Johnson, S. P. Daley, and S. T. Ceyer, Faraday Discuss. Chem. Soc. **91**, 437 (1991).
[26] J. E. Hurst, C. A. Becker, J. P. Cowin, K. C. Janda, L. Wharton, and D. J. Auerbach, Phys. Rev. Lett. **43**, 1175 (1979).